Long-Term Orbital Evolution of Binary Systems Interacting with Circumbinary Disks

Project report for the MPA-Kavli Summer Program 2023

RUGGERO VALLI[1]

[1]*Max-Planck-Institut für Astrophysik, Karl-Schwarzschild-Straße 1, 85741 Garching, Germany*

Advisors:
Christopher Tiede
Jorge Cuadra
Selma E. de Mink
Alejandro Vigna-Gómez

1. INTRODUCTION

Circumbinary disks are ubiquitous in the universe, appearing at different scales from supermassive black holes (Begelman et al. 1980; Escala et al. 2005; Roedig et al. 2011; Franchini et al. 2021) to star formation (Dutrey et al. 1994; Mathieu et al. 1997; Tofflemire et al. 2017; Long et al. 2021) to post-AGB (Deroo et al. 2007; Mohamed & Podsiadlowski 2012) and post-CE systems (Kashi & Soker 2011; Reichardt et al. 2019; Röpke & De Marco 2023; Tuna & Metzger 2023). One of the major challenges in the study of circumbinary disks is understanding how the interaction with the disk will influence the orbital evolution of the binary. The intricate interplay between the binary and the disk can lead to a wide array of outcomes, including changes in orbital separation, eccentricity, and even mergers.

A substantial body of research, spanning from early analytical and numerical investigations (Artymowicz 1983; Artymowicz et al. 1991; Pringle 1991) to more recent numerical simulations (e.g., Shi et al. 2012; Tang et al. 2017; Muñoz et al. 2020) reveals the strong sensitivity of these outcomes to the system's parameters. Consequently, the current understanding delineates a complicated landscape within a parameter space that remained, until recently, relatively uncharted. The evolution of the orbital parameters is a non-trivial function of eccentricity (Zrake et al. 2021; Siwek et al. 2023a) and mass ratio (Ragusa et al. 2020; Duffell et al. 2020; Siwek et al. 2023b,a), and can also be influenced by disk aspect ratio (Tiede et al. 2020; Dittmann & Ryan 2022), viscosity (Duffell et al. 2020; Dittmann & Ryan 2022) and disk-orbit inclination (Moody et al. 2019; Smallwood et al. 2022; Tiede & D'Orazio 2023).

The sensitivity to system parameters necessitates extensive parameter exploration studies, as seen in prior works such as Zrake et al. (2021); D'Orazio & Duffell (2021); Siwek et al. (2023b,a), which are computationally demanding, thus limiting the ability to follow the long-term evolution of the system. Indeed, the strategy often adopted in numerical simulations of circumbinary disks is to keep the orbit of the binary fixed and only compute the torques acting on it, thereby providing derivatives of the orbital parameters.

In this work, we compute the long-term evolution of binary systems interacting with circumbinary disks by integrating derivatives obtained from the literature, specifically those by Siwek et al. (2023b,a), and Zrake et al. (2021). In Section 3.1 we show the possible evolutionary paths in the eccentricity, mass ratio and orbital separation, and describe the equilibrium configurations and the attractor points. In Section 3.2 we examine the evolution of a population of systems and identify potential observational signatures arising from interactions with circumbinary disks. In Section 4 we discuss astrophysical applications of our findings. Lastly, we summarize the results in Section 5.

2. METHODS

2.1. *Hydrodynamic simulations of circumbinary disks*

We employ the results of two sets of hydrodynamic simulations: The first set (hereafter model S), was carried out by Siwek et al. (2023a,b) using the moving-mesh code `AREPO` (Springel 2010; Pakmor et al. 2016; Muñoz & Lai 2016). The second set (hereafter model Z), was conducted by Zrake et al. (2021) with the grid-based code `Mara3` (Zrake & MacFadyen 2012; Tiede et al. 2020). Here, we provide an overview of the key assumptions underlying these simulations.

Both simulations represent a finite gas disk accreting onto a central binary on a coplanar prograde orbit. The two objects composing the binary were modelled as sink particles of mass M_1 and M_2 (where $M_1 > M_2$) and total mass $M = M_1 + M_2$. The mass of the disk was taken to be much smaller than the mass of the binary so that the self-gravity of the disk could be ignored. These simulations aimed to capture the regime where the objects' radii are substantially smaller than their separation. Although the numerical sink radii were larger than the actual object radii, they remained considerably smaller than the orbital separation. Both models employed a locally isothermal equation of state, maintaining vertical hydrostatic equilibrium, effectively reducing the equations to a 2D problem. The disk aspect ratio was set to $h/r = 0.1$, where h is the thickness of the disk and r is the radial coordinate. This value falls within the range expected for accretion disks around stellar-mass objects. We can show this via an estimate given by equation 2.19 of Shakura & Sunyaev (1973), which, for parameters typical of an accreting stellar binary gives

$$h/r \approx 0.12 \left(\frac{M}{\mathrm{M}_\odot}\right)^{-3/8} \left(\frac{r}{\mathrm{AU}}\right)^{1/8} \left(\frac{\alpha}{0.1}\right)^{-1/10} \left(\frac{\dot{M}}{10^{-6}\,\mathrm{M}_\odot\,\mathrm{yr}^{-1}}\right)^{3/20}, \quad (1)$$

where M is the mass of the central object (in this context, the total mass of the binary), r is the radial coordinate of the disk, to be taken as comparable to the size of the circumbinary cavity, α is the Shakura-Sunyaev viscosity parameter and $\dot{M}$ is the mass accretion rate.

However, when rewriting Equation 1 for parameters typical of supermassive black holes, a significantly lower aspect ratio is obtained.

$$h/r \approx 3.9 \times 10^{-3} \left(\frac{M}{10^8\,\mathrm{M}_\odot}\right)^{-1/10} \left(\frac{r}{10^4\,r_g}\right)^{1/8} \left(\frac{\alpha}{0.1}\right)^{-1/10} \left(\frac{L}{L_{\mathrm{Edd}}}\right)^{3/20} \left(\frac{\eta}{0.06}\right)^{-3/20}, \quad (2)$$

where $r_g = \frac{2GM}{c^2}$ is the Schwarzschild radius, $L = \eta \dot{M} c^2$ is the disk luminosity, η is the gravitational energy release efficiency, and $L_{\rm Edd}$ is the Eddington luminosity. Considering the weak dependence of the disk aspect ratio on all the parameters involved, the observation that h/r significantly differs between supermassive black hole binaries and stellar binaries remains robust, even when subjected to minor parameter variations.

The two models considered in this work use an α-viscosity prescription with $\alpha = 0.1$. As shown by Tiede et al. (2020); Dittmann & Ryan (2022), for the assumed aspect ratio the choice of viscosity does not have a large impact on the evolution of the orbital parameters.

Under the stated assumptions, the system of equations that was solved becomes scale-free, and the only parameters left to fix are the binary mass ratio $q = M_2/M_1$ and the eccentricity of the binary orbit e.

While the two models share similar physical assumptions, they explore the eccentricity-mass ratio parameter space in different ways. Model S is based on rectangular grids of simulations considering 10 mass ratio values within the range $0.1 \leq q \leq 1$, and 5 values of orbital eccentricity in Siwek et al. (2023b) and 8 values in Siwek et al. (2023a), spanning from $e = 0$ to $e = 0.8$ in both cases. Conversely, model Z is based on simulations of equal mass binaries $q = 1$, that cover $0 \leq e \leq 0.8$ with a finer grid of 33 points.

For each combination of e and q, the evolution of the disk was followed — while keeping the orbit of the binary fixed — for several viscous times $t_{\rm visc}$ until the disk was deemed relaxed and the mass accretion rate had reached a steady state. The total torque acting on the binary is computed in post-processing, taking into account the gravitational torque from the gas distribution and the accretion of angular momentum on the sink particles. From the torque, the derivative of the parameters of the binary are computed and averaged over a number of orbits sufficient to remove the effect of the orbital variability and the variability associated with the circumbinary disk precession. These measurements are valid in the limit where the parameters of the binary vary on a timescale much longer than the relaxation time of the disk, that is when $X/\dot{X} \gg t_{\rm visc}$, where X stands for semimajor axis a, eccentricity e or mass ratio q.

Figure 1 compares both models in the regime $q = 1$. The values on the y-axis are in units of $\dot{M}/M$, which can also be expressed as

$$\frac{\dot{a}/a}{\dot{M}/M} = \frac{\mathrm{d}\log a}{\mathrm{d}\log M},$$
$$\frac{\dot{e}}{\dot{M}/M} = \frac{\mathrm{d}e}{\mathrm{d}\log M}.$$

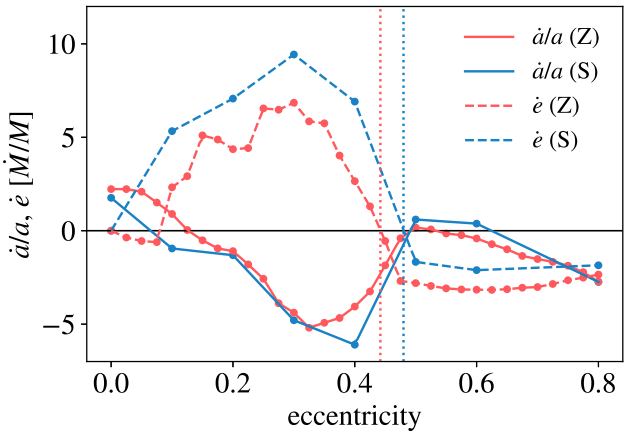

Figure 1. Comparison of the results of hydro simulations (model Z in red and model S in blue) showing the relative rate of change of the separation ($\dot{a}/a$, solid line) and eccentricity ($\dot{e}$, dashed line) due to the presence and interaction with a circumbinary disk. Results are shown for different eccentricities (x-axis) and assuming equal masses ($q = 1$). The y-axis is in units of $\dot{M}/M$. The vertical lines indicate the equilibrium eccentricities of the two models.

The choice of these units is convenient because in this way the quantities are invariant under re-scaling of the simulation's physical units of binary mass and gas surface density.

The predictions of the two models broadly agree, showing a similar trend and an equilibrium eccentricity around $e \approx 0.5$ (see Roedig et al. 2011, for a simple explanation of the presence of an equilibrium eccentricity). However, model S finds a positive $\dot{e}$ for all eccentricities below the equilibrium value, while model Z predicts that systems with $e \lesssim 0.1$ will tend to circularize. A negative $\dot{e}$ was also found by Duffell et al. (2020); D'Orazio & Duffell (2021), while other studies find a positive $\dot{e}$ for $e \leq 0.2$ (e.g., Artymowicz et al. 1991; Cuadra et al. 2009; Roedig et al. 2011). The reason for this discrepancy is currently unclear. Siwek et al. (2023a) attributes it to the different radial dependency of the kinematic viscosity adopted for instance by D'Orazio & Duffell (2021), but this cannot explain how Siwek et al. (2023a) and Zrake et al. (2021) — who adopt the same viscosity prescription — obtain a different result.

2.2. *Integration of the orbital evolution*

To compute the long-term orbital evolution of the binary systems, we interpolate the derivatives of the binary parameters obtained from the hydrodynamic simulations and integrate them as a function of the accreted mass.

To achieve this, we define a set of functions that linearly interpolate the derivatives provided by the two hydrodynamic models.

Regarding model S, we use bilinear interpolation on the rectangular grid to obtain the functions $f_a^{(S)}(e, q)$ and $f_e^{(S)}(e, q)$, which interpolate the values in Figure 2 and 3 of

Siwek et al. (2023a), while

$$f_q^{(S)}(e,q) = \frac{(1+q)(\lambda(e,q)-q)}{1+\lambda(e,q)}, \tag{3}$$

where $\lambda(e,q)$ interpolates the values in Figure 4 of Siwek et al. (2023b). These functions are defined for $0 \leq e \leq 0.8$ and $0.1 \leq q \leq 1$.

For model Z, we define $f_a^{(Z)}(e,q)$ and $f_e^{(Z)}(e,q)$ as linear interpolants of the values in Figure 1 and $f_q^{(Z)}(e,q) = 0$. These functions are defined for $0 \leq e \leq 0.8$ and $q = 1$.

The evolution of the binary system is then determined by solving the differential equations

$$\frac{\mathrm{d}\log a}{\mathrm{d}\log M} = f_a(e,q), \tag{4}$$

$$\frac{\mathrm{d}e}{\mathrm{d}\log M} = f_e(e,q), \tag{5}$$

$$\frac{\mathrm{d}q}{\mathrm{d}\log M} = f_q(e,q), \tag{6}$$

with appropriate initial conditions e_0 and q_0. Given the scale invariance of the problem, we always set $a_0 = 1$. We report the tables of the values on which the interpolations are based in Appendix A.

3. RESULTS

3.1. *Trajectories in q-e-a space*

Figure 2 is a map of the flow of the above equations for model S in the q-e space. Each streamline represents a possible evolution of a system interacting with a circumbinary disk. The visualization highlights the presence of an equilibrium eccentricity that varies weakly as a function of mass ratio. Eccentricity is more easily changed than mass ratio, therefore the evolution can be regarded as composed of two phases. In the first phase, eccentricity evolves towards the equilibrium value, keeping the mass ratio almost constant. In the second phase, the mass ratio moves towards unity, while the eccentricity is maintained at the equilibrium value as it changes with mass ratio.

If the process were to continue indefinitely, all the streamlines would converge to the single attractor at $q = 1$ and $e \approx 0.5$, where there is a small, but non-zero negative $\dot{a}$. A system that accretes matter indefinitely would then keep reducing the orbital separation until tides, gravitational waves or other processes would take over. However, it is not guaranteed that a realistic binary will reach the attractor in the first place, because either the circumbinary disk will at some point be depleted or other physical mechanisms will come into play and dominate the evolution of the orbit.

The thickness and colour of the streamlines encode the velocity of the flow, which tends to be faster in the bottom region of Figure 2, where the eccentricity is below the equilibrium value. It has already been observed that systems with higher e need to accrete more mass to change q (Dunhill et al. 2015; Siwek et al. 2023b). Figure 2 shows that systems with higher e are slower to change eccentricity as well.

Model Z presents one important difference: since circular orbits are unstable in model S but stable in model Z, model Z predicts a second stable point at $q = 1$ and $e = 0$ with positive $\dot{a}$ (see Figure 1 of Zrake et al. 2021). Model Z is only applicable when $q = 1$. However, multiple groups found that $\frac{\mathrm{d}q}{\mathrm{d}\log M} \geq 0$ in most configurations (Lubow & D'Angelo 2006; Farris et al. 2014; Duffell et al. 2020; Siwek et al. 2023a, but see Dunhill et al. 2015, which find an equal or greater accretion rate on the more massive object) which would make ($q = 1$, $e = 0$) a second global attractor.

Figures 3 and 4 show how the eccentricity and semimajor axis change as a function of the amount of accreted mass for model S and model Z, respectively. The eccentricity is the first property to change. It reaches the equilibrium value after the system has accreted $\approx 10\%$ of its original mass. Subsequently, the evolution in eccentricity proceeds more slowly, following the equilibrium value as the mass ratio changes.

Despite the presence of several regions of the e-q parameter space with a positive $\dot{a}$, according to model S, the orbit will generally tend to shrink, regardless of initial conditions. However, in order to achieve a significant reduction of the orbital separation $\Delta a \approx a_0$ the system needs to accrete from the disk an amount of mass comparable to the initial mass of the system $\Delta M \approx M_0$. This implies that the interaction with a circumbinary disk may not be a viable mechanism to reduce the orbital separation if the gas reservoir that can potentially be accreted is smaller than the total mass of the binary.

The behaviour is different for model Z, for which the long-term evolution of the orbit is sensitive to the initial eccentricity. If $e_0 \lesssim 0.1$ the orbit will circularize and widen, while if $e_0 \gtrsim 0.1$ the eccentricity will increase up to $e \approx 0.5$ and then the orbit will shrink. A small discrepancy in the prediction of the two models for $\dot{e}$ when $e \lesssim 0.1$ leads to a dramatically different long-term evolution.

Comparing Figure 4 with the bottom right panel of Figure 3 it is clear that the change in orbital separation predicted by model Z after accreting $\Delta M/M \approx 2$ is significantly larger than in model S. This is due to a different value of $\dot{a}/a$ at the equilibrium eccentricity in the two models. In Figure 5 we show this value as a function of mass ratio. For $q = 1$, model S predicts $\dot{a}/a|_{e=e_{\mathrm{eq}}} \approx -0.7$, while according to model Z $\dot{a}/a|_{e=e_{\mathrm{eq}}} \approx -2.3$, resulting in a smaller orbital separation for the same accreted mass. As a further note, D'Orazio & Duffell (2021) find a value compatible with zero but conclude that systems oscillating around the equilibrium eccentricity would experience a net orbital shrinkage. To determine whether binary-disk interactions are a viable mechanism to shrink the orbit in realistic astrophysical situations,

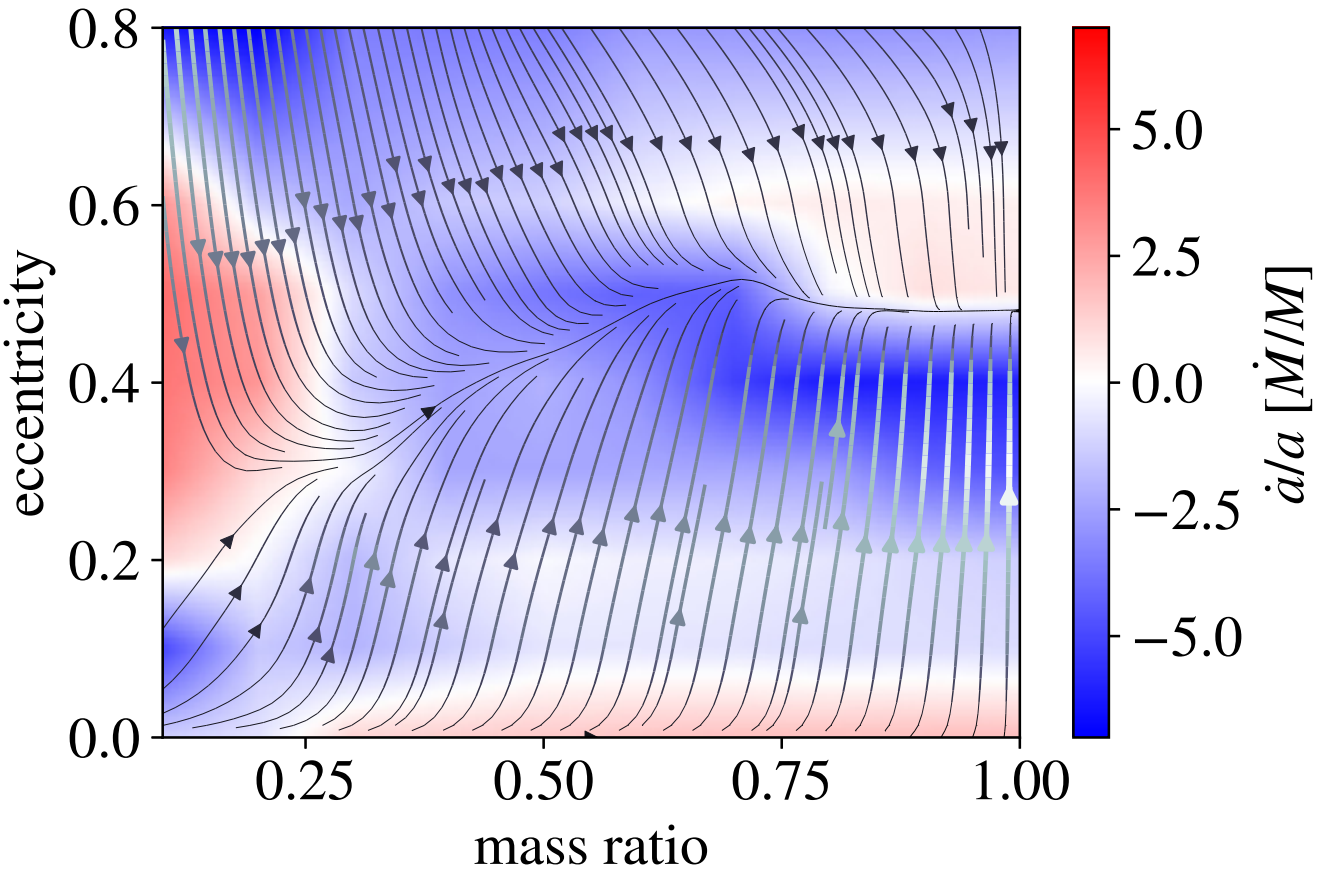

Figure 2. In the foreground, the flow of Equations 5 and 6 for model S. The streamlines are tangential to the derivative vector field ($\dot{q}$, $\dot{e}$) at each point. Thicker streamlines (and with a lighter colour) correspond to a faster flow. Each streamline coincides with a possible trajectory in the (q,e) space of a system that accretes from a circumbinary disk. The background colour shows the derivative of the orbital separation $\dot{a}/a$ in units of $\dot{M}/M$ (Equation 4). Blue regions correspond to orbital shrinking, while red regions to orbital widening.

it will be necessary to constrain the asymptotic value of $\dot{a}/a$ more precisely.

3.2. *Population evolution*

In this section, we show the effect of circumbinary disks on a population of binaries and describe the signatures that they produce on the distribution of orbital parameters. We randomly sample a population of binary systems from some initial parameter distribution and then compute the orbital and mass ratio evolution forward in time, assuming that each system is accreting from a circumbinary disk.

The best choice of initial parameters distribution depends on the application: whether we consider the binary-disk interaction during the star formation process, during the post-plunge-in phase of a common envelope event, or for Super Massive Black Hole (SMBH) binaries, the initial distribution of eccentricity and mass ratio can be very different and in all cases highly uncertain. See e.g., Offner et al. (2022); Elsender et al. (2023); Tokovinin & Moe (2020) for binaries during star formation, Trani et al. (2022); Gagnier & Pejcha (2023); Tuna & Metzger (2023); Kruckow et al. (2021) for post–common-envelope systems and Begelman et al. (1980); Sesana & Khan (2015); del Valle et al. (2015); Goicovic et al. (2017); Bortolas et al. (2021) for SMBH binaries.

Even though the initial parameter distribution depends on the specific application and can be highly uncertain, the fast convergence of the solutions to the attractors guarantees a weak dependence on the initial conditions. Therefore we rely on simple initial distributions, namely a flat distribution of eccentricity between $0 \leq e_0 \leq 0.8$ and a flat distribution in mass ratio between $0.1 \leq q_0 \leq 1$. Since the problem is scale-free, we do not need to specify a value for the initial separation a_0, and we parameterize the accreted mass in terms of the initial mass M_0.

Figure 6 shows the evolution of 10^4 systems of this population according to model S. Up to the accretion of $\approx 10\%$ of the initial mass in the binary ($\Delta M/M_0 \leq 0.1$), the most noticeable variation happens in the eccentricity distribution in the top panel, which concentrates around $e \approx 0.5$. For $\Delta M/M_0 \geq 0.5$ there is also a significant evolution in the

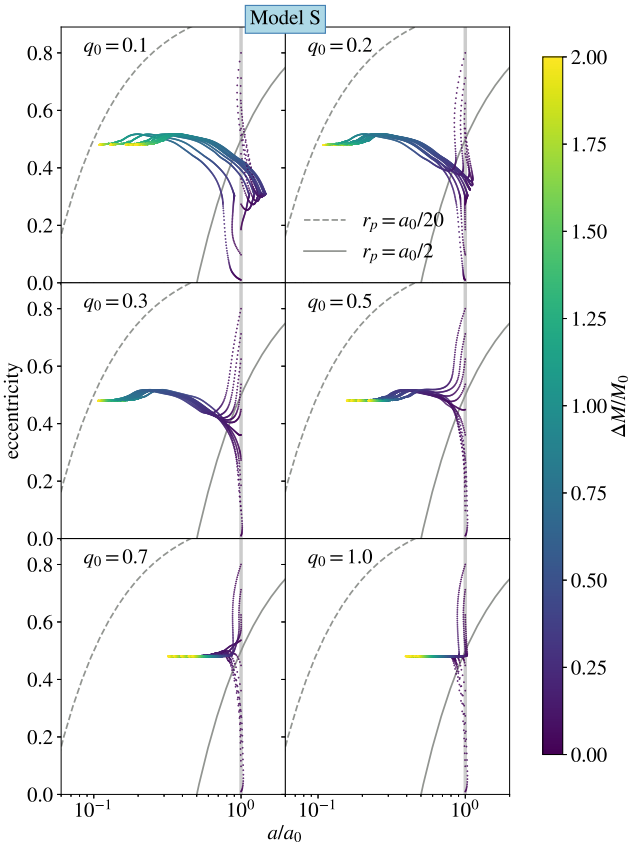

Figure 3. Evolution of eccentricity e and semimajor axis a according to model S. For each panel, the systems start from a different initial mass ratio q_0 from 0.1 (top left) to 1.0 (bottom right). Within each panel, the initial eccentricity e_0 spans from 0.01 to 0.8. The trajectories are coloured based on the mass change $\Delta M/M_0$, where M_0 is the initial mass of the binary and ΔM is the amount of accreted mass. All the systems start along the vertical line $a = a_0$, highlighted in with a thick grey line. The two thin grey curves indicate where the orbital periastron distance is 0.5 (solid) or 0.05 (dashed) times the initial semimajor axis.

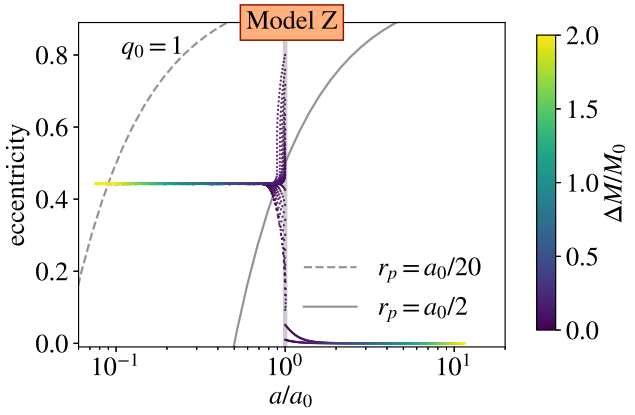

Figure 4. Same as in figure 3, but for model Z, and only for the case $q_0 = 1$.

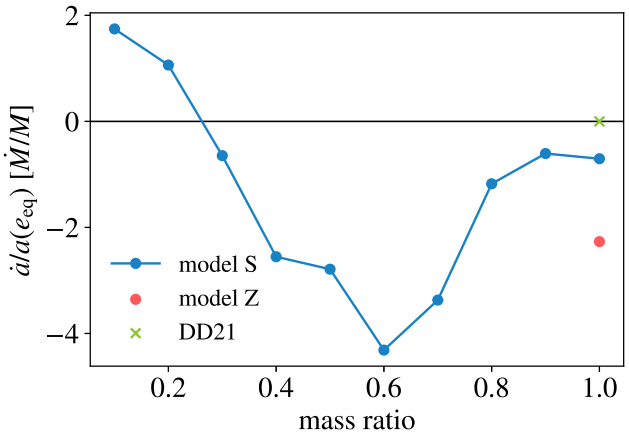

Figure 5. Rate of separation change $\dot{a}/a$ computed at the equilibrium eccentricity, as a function of mass ratio. Model S is in blue, and model Z is in red. For comparison, we report the result of D'Orazio & Duffell (2021) marked with a green x.

distribution of mass ratio — that starts to peak at $q = 1$ as mass ratios below $q = 0.5$ are depopulated — and of semimajor axis a/a_0, which becomes ≈ 0.6 dex broad and double-peaked, since the systems that start with $q < 0.8$ migrate to a smaller orbit faster (see Figure 5) but slow down and accumulate on the left peak once they reach equal mass ratio.

Figure 7 shows the same evolution but for model Z, assuming that all the systems start at $q_0 = 1$. The top panel highlights how the distribution of eccentricity evolves towards a bimodal configuration (the two peaks corresponding to the two attractors of the differential equations) as a gap at $e \approx 0.1$ forms already after accreting 5% of the initial mass (cf. Figure 1 of Zrake et al. 2021). The bottom panel shows the distribution of the semimajor axis with respect to the initial value a_0. After accreting 50% of the initial mass, two populations appear in the distribution, corresponding to the two attractors.

Figure 8 depicts the evolution of the population in the e-q plane according to model S. In the top-left panel, every system has accreted 1% of the initial mass, and this is not sufficient to alter the distribution of eccentricity and mass ratio significantly, which remains close to the initial flat distribution. After accreting 5% of the initial mass — in the top-right panel — a pattern starts to emerge and becomes evident in the middle-left panel as a clear correlation between eccentricity and mass ratio, caused by the accumulation of systems close to their equilibrium eccentricity. When the systems have accreted 20% of the initial mass (middle-right panel) the correlation becomes extremely tight. In the remaining two panels, after accreting 50% or 100% of the initial mass, all the systems settle at the same eccentricity $e \approx 0.5$ and move towards an equal mass ratio. This e-q correlation could be observed in

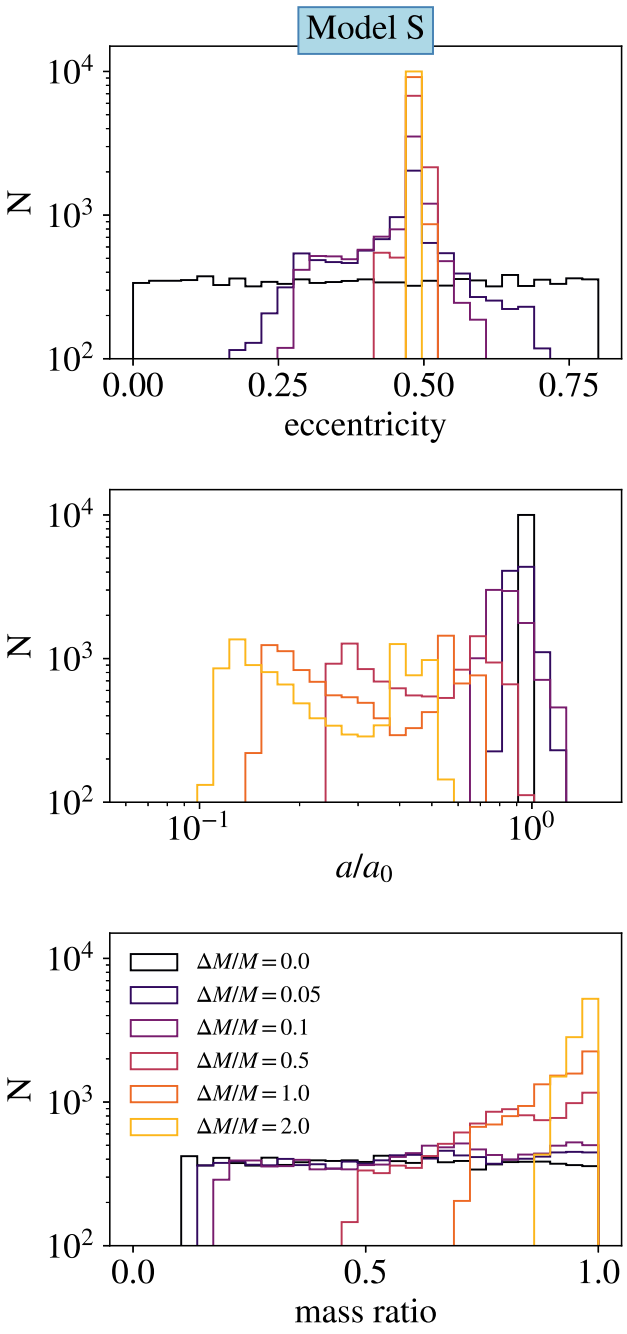

Figure 6. Distribution of eccentricity (top), semimajor axis (middle) and mass ratio (bottom) for a population of 10^4 binaries, according to model S. Each colour corresponds to a different amount of accreted mass.

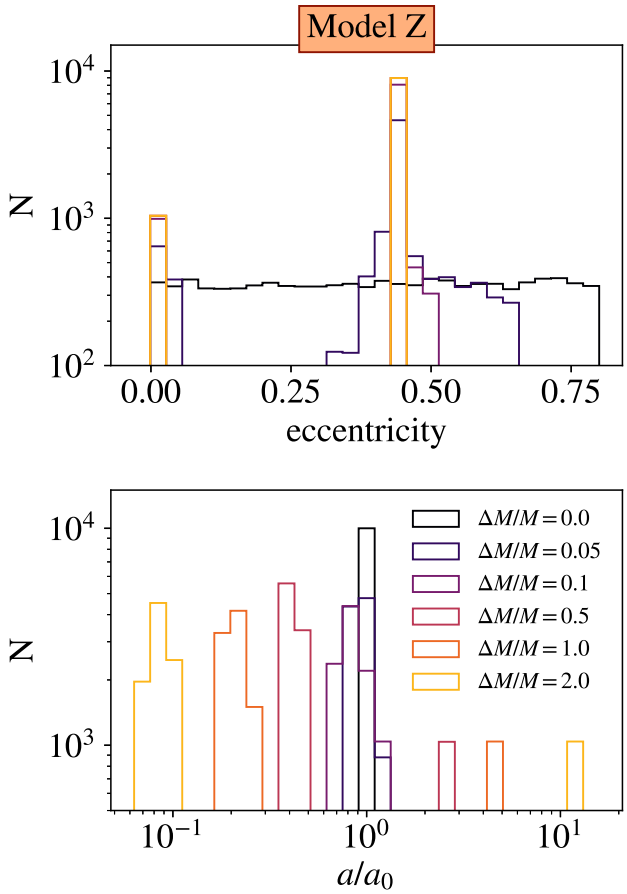

Figure 7. As in figure 6, but for model Z. Only the panels with eccentricity (top) and semimajor axis (bottom) are shown.

populations of binaries that have undergone steady accretion from a circumbinary disk in the past, and whose orbit has not since been modified through other means. The presence of the correlation can also help constrain the typical amount of mass that was accreted from the disk.

4. ASTROPHYSICAL IMPLICATIONS

We have investigated the long-term orbital evolution of binary systems subjected to the accretion of a circumbinary gas disk, by employing the results of two suits of 2D hydrodynamic simulations. The scale-free nature of these simulations allows for a broad applicability, encompassing a diverse range of astrophysical scenarios, including binary star formation, post–common-envelope systems, and binary supermassive black holes. Our results provide insights into the complex interplay between the binary system and its surrounding disk, yielding valuable outcomes regarding the evolution of orbital parameters. We discuss here the astrophysical and observational implications and describe how these results can help guide the direction of future efforts and advancements in the field.

4.1. *Binary Star Formation*

One proposed mechanism for the formation of close binary stars (see Offner et al. 2022, for a review) revolves around the concept of disk fragmentation (Adams et al. 1989; Shu et al. 1990; Bonnell & Bate 1994; Mignon-Risse et al. 2023). According to this model, fragments within the disk grow and undergo inward migration (Ward 1997; Kley & Nelson 2012),

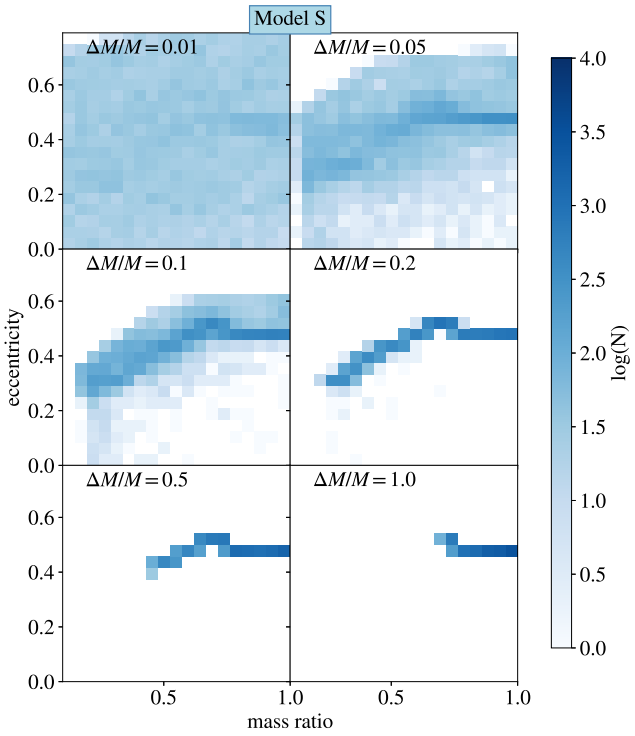

Figure 8. Distribution of the systems in the e-q plane for a population evolving according to model S. Each panel corresponds to a different amount of accreted mass, increasing from top-left to bottom-right. The colour scale indicates the number of systems falling into each bin.

ultimately leading to the formation of a central gas cavity around the two young stellar objects. Binaries have been observed in this regime (Andrews et al. 2014; Lacour et al. 2016; Long et al. 2021), showing evidence of interaction between the binary and the disk (Price et al. 2018; Aly et al. 2018).

If, following the formation of the cavity, the subsequent orbital evolution is primarily governed by a sustained interaction with a thin, stable accretion disk, we should anticipate the emergence of observable signatures of this interaction within the measured distributions of eccentricity and mass ratio among main sequence stars. Particularly, this signature should be evident in binary systems with sufficiently wide orbits, which have remained unaltered by tides during their main sequence phase.

Regarding model S, we expect a clear correlation between eccentricity and mass ratio, as illustrated in Figure 8. Conversely, for model Z we predict the presence of a distinct gap in the eccentricity distribution, occurring around $e \approx 0.1$ (see Figure 1 of Zrake et al. (2021)).

It is important to note that these characteristic signatures would remain observable even if steady accretion from a disk is not the dominant process (the accretion might be bursty. e.g., Hartmann & Kenyon 1996; Tokovinin & Moe 2020; Elbakyan et al. 2021), as long as at least the final few per cent of the mass is accreted with conditions aligned to the ones considered in this work. To our knowledge, such features in the main sequence star populations have not been reported in the literature (Tokovinin 2020; Hwang et al. 2022; Andrew et al. 2022; Gaia Collaboration et al. 2023). This suggests that either mass accretion from a thin, stable disk accounts for less than 1% of the mass of the binary, or there might be some physical processes (such as outflows, radiation transport or dynamical interactions with other stars) that are currently not included in the circumbinary disk models but will turn out to be essential for the orbital evolution of young stellar objects.

Interaction of massive binary stars with a disk has been also hypothesized as a possible mechanism to explain the observed increase of radial velocity dispersion in young clusters as they age (Sana et al. 2017; Ramírez-Tannus et al. 2017, 2020, 2021). However, it is worth noting that explaining the considerable decrease in the minimum period, from $3500\,\mathrm{d}$ in M17 to $1.4\,\mathrm{d}$ in the older clusters, a binary with an initial total mass of $M = 20\,\mathrm{M}_\odot$, would require a shrinkage of the semimajor axis of approximately 200 times. Based on our current findings, achieving such a significant reduction would require the system to accrete from the disk an amount of mass several times larger than the initial mass of the binary, a scenario that is deemed unlikely to occur.

4.2. *Post-Interaction Binaries*

Another scenario wherein the interaction with a circumbinary disk may play a crucial role is during the late phases of a common envelope. 3D simulations have shown that following the initial dynamical phase of plunge-in, the inspiral process may stall, even if the envelope has not been completely ejected, due to the formation of a low gas-density region at the envelope's centre, which inhibits dynamical friction (Passy et al. 2012; Ricker & Taam 2012; Ricker et al. 2019; Lau et al. 2022b,a). Subsequently, the bound part of the remaining envelope can cool and form a centrifugally supported disk, a process computationally difficult to treat due to the longer timescales involved (but see Gagnier & Pejcha 2023). The interaction of the binary with the disk has been proposed as a mechanism to further reduce the orbital separation (Kashi & Soker 2011; Tuna & Metzger 2023) and potentially lead to a late merger. Consequently, the final state of the system would be influenced significantly by the interaction with the disk, carrying crucial implications for compact object mergers and gravitational wave rates (Belczynski et al. 2007; Stevenson et al. 2017).

In the present study, we offer quantitative predictions for the effect of the disk's interaction with the orbit in the post-plunge-in phase of a common envelope event. It is expected that when the plunge-in stalls, the orbit will be nearly circular (although a small residual eccentricity may persist, e.g.,

Trani et al. 2022). In such a case, the two models considered in our work predict substantially different outcomes for the subsequent evolution. According to model Z, systems with low residual eccentricity will become more circular, but their orbits will widen instead of shrinking. On the other hand, model S predicts that the orbit of the systems will shrink, but only after their eccentricity has been excited to $e \approx 0.5$. However, observed post-common-envelope candidates appear to favour small eccentricities (Kruckow et al. 2021) and this fact cannot be explained by a process of tidal circularization successive to the interaction with the disk. Indeed, we can employ the tidal synchronization timescale from (Campbell 1984) as a lower bound on the time required for the orbit of a double white dwarf system to circularize.

$$t_{\rm circ} > t_{\rm sync} = 7 \times 10^6 \,{\rm Gyr} \left(\frac{P}{0.01\,{\rm d}}\right)^4 \left(\frac{R_1}{1\times10^4\,{\rm km}}\right)^{-6} \left(\frac{M_1/0.5\,{\rm M}_\odot}{L_1/0.001\,{\rm L}_\odot}\right)^{5/7} \left(\frac{M_1}{M_2}\right)^2, \tag{7}$$

where P is the orbital period, R_1, M_1 and L_1 are the radius, mass and luminosity of the white dwarf for which we are computing the tidal dissipation, and M_2 is the mass of the companion. For typical values of post–common-envelope double white dwarf systems, this timescale far exceeds the age of the universe.

In conclusion, neither model Z nor model S seems to be able to provide a mechanism to reduce the orbital separation while maintaining consistency with the observed low eccentricities of post-common-envelope systems.

4.3. *Supermassive Black Hole Binaries*

The simulations underlying this work assume a disk aspect ratio of $h/r = 0.1$, which is notably higher than the typical values of $h/r \approx 10^{-2} - 10^{-3}$ expected for accreting supermassive black holes (see Equation 2). Simulating the low aspect ratio regime poses numerical challenges, but it may present important differences with the $h/r = 0.1$ case. Tiede et al. (2020) showed that changing h/r can dramatically alter the outcome of the interaction with the disk, transitioning from expansion to contraction of the orbit, while Dittmann & Ryan (2022) established that at lower h/r values, the orbital evolution becomes sensitive to the treatment of viscosity. For these reasons, we refrain from giving a quantitative statement on the evolution of supermassive black hole binaries interacting with a disk. Nonetheless, if a similar eccentricity attractor exists within this regime, we would expect supermassive black hole binaries to maintain a relatively large eccentricity $e \sim 0.5$, which could be detected in electromagnetic searches. This eccentricity will decrease once gravitational wave emission starts dominating the orbital evolution, but a detectable non-zero residual eccentricity should still be present when entering the LISA band (Roedig et al. 2011).

5. CONCLUSION

In this study, we explore the long-term orbital evolution of binary systems interacting with circumbinary disks, accounting for both eccentricity and mass ratio changes. Our findings can be summarized as follows:

- To alter significantly the orbital separation, the system needs to accrete a mass comparable to the total mass of the binary.
- If the initial eccentricity is exceeds about 0.1, two consistent trends emerge:
  - After accreting $\approx 10\%$ of the initial mass, the eccentricity will stabilize at an equilibrium value $e \approx 0.5$ that depends weekly on the mass ratio.
  - After accreting a mass comparable to the mass of the binary, the orbital separation will shrink appreciably.
- For initial eccentricities below approximately 0.1, our two models yield contrasting predictions. Model Z predicts that the orbit will circularize and then widen, while model S suggests that the eccentricity will be excited to $e \approx 0.5$, and then the orbit will shrink. The difference between the two predictions hinges on the different sign of $\dot{e}$ when $e < 0.1$.

As a consequence of the above findings, a population of binaries that are interacting (or have recently interacted) with a thin, stable circumbinary disk will show some clear signatures in the orbital parameters distributions:

- Model S: a correlation between mass ratio and eccentricity.
- Model Z: a gap in the eccentricity distribution at $e \approx 0.1$.

If thin, stable circumbinary disk accretion happens in the last stages of binary star formation, these signatures could manifest in populations of main sequence stars that have an orbit wide enough that tidal circularization is negligible. Similarly, disk interactions could leave an imprint on the orbit of post–common-envelope systems, even though we have shown that none of the two models here discussed are able to explain the small eccentricity observed while at the same time providing a viable mechanism to shrink the orbit the after the plunge-in phase. Lastly, our findings suggest that supermassive black hole binaries may often display a relatively large eccentricity, that could be measured in electromagnetic searches, as well as a small residual eccentricity

in future gravitational wave detections of supermassive black hole mergers.

ACKNOWLEDGMENTS

RV thanks Paul Ricker, Norbert Langer, Shazrene Mohamed, Carlos Badenes and all the participants to the MPA-Kavli Summer Program 2023 for the useful discussions. The authors acknowledge the Max Planck Institute for Astrophysics and the Kavli Foundation for supporting the MPA-Kavli Summer Program 2023, during which this project was conducted.

REFERENCES

Adams, F. C., Ruden, S. P., & Shu, F. H. 1989, ApJ, 347, 959, doi: 10.1086/168187

Aly, H., Lodato, G., & Cazzoletti, P. 2018, MNRAS, 480, 4738, doi: 10.1093/mnras/sty2179

Andrew, S., Penoyre, Z., Belokurov, V., Evans, N. W., & Oh, S. 2022, MNRAS, 516, 3661, doi: 10.1093/mnras/stac2532

Andrews, S. M., Chandler, C. J., Isella, A., et al. 2014, ApJ, 787, 148, doi: 10.1088/0004-637X/787/2/148

Artymowicz, P. 1983, Acta Astronomica, 33, 223. https://ui.adsabs.harvard.edu/abs/1983AcA....33..223A

Artymowicz, P., Clarke, C. J., Lubow, S. H., & Pringle, J. E. 1991, ApJL, 370, L35, doi: 10.1086/185971

Begelman, M. C., Blandford, R. D., & Rees, M. J. 1980, Nature, 287, 307, doi: 10.1038/287307a0

Belczynski, K., Taam, R. E., Kalogera, V., Rasio, F. A., & Bulik, T. 2007, ApJ, 662, 504, doi: 10.1086/513562

Bonnell, I. A., & Bate, M. R. 1994, MNRAS, 271, 999, doi: 10.1093/mnras/271.4.999

Bortolas, E., Franchini, A., Bonetti, M., & Sesana, A. 2021, ApJL, 918, L15, doi: 10.3847/2041-8213/ac1c0c

Campbell, C. G. 1984, MNRAS, 207, 433, doi: 10.1093/mnras/207.3.433

Cuadra, J., Armitage, P. J., Alexander, R. D., & Begelman, M. C. 2009, MNRAS, 393, 1423, doi: 10.1111/j.1365-2966.2008.14147.x

del Valle, L., Escala, A., Maureira-Fredes, C., et al. 2015, ApJ, 811, 59, doi: 10.1088/0004-637X/811/1/59

Deroo, P., Acke, B., Verhoelst, T., et al. 2007, A&A, 474, L45, doi: 10.1051/0004-6361:20078079

Dittmann, A. J., & Ryan, G. 2022, MNRAS, 513, 6158, doi: 10.1093/mnras/stac935

D'Orazio, D. J., & Duffell, P. C. 2021, ApJ, 914, L21, doi: 10.3847/2041-8213/ac0621

Duffell, P. C., D'Orazio, D., Derdzinski, A., et al. 2020, ApJ, 901, 25, doi: 10.3847/1538-4357/abab95

Dunhill, A. C., Cuadra, J., & Dougados, C. 2015, MNRAS, 448, 3545, doi: 10.1093/mnras/stv284

Dutrey, A., Guilloteau, S., & Simon, M. 1994, A&A, 286, 149. https://ui.adsabs.harvard.edu/abs/1994A&A...286..149D

Elbakyan, V. G., Nayakshin, S., Vorobyov, E. I., Caratti O Garatti, A., & Eislöffel, J. 2021, A&A, 651, L3, doi: 10.1051/0004-6361/202140871

Elsender, D., Bate, M. R., Lakeland, B. S., Jensen, E. L. N., & Lubow, S. H. 2023, MNRAS, 523, 4353, doi: 10.1093/mnras/stad1695

Escala, A., Larson, R. B., Coppi, P. S., & Mardones, D. 2005, ApJ, 630, 152, doi: 10.1086/431747

Farris, B. D., Duffell, P., MacFadyen, A. I., & Haiman, Z. 2014, ApJ, 783, 134, doi: 10.1088/0004-637X/783/2/134

Franchini, A., Sesana, A., & Dotti, M. 2021, MNRAS, 507, 1458, doi: 10.1093/mnras/stab2234

Gagnier, D., & Pejcha, O. 2023, A&A, 674, A121, doi: 10.1051/0004-6361/202346057

Gaia Collaboration, Arenou, F., Babusiaux, C., et al. 2023, A&A, 674, A34, doi: 10.1051/0004-6361/202243782

Goicovic, F. G., Sesana, A., Cuadra, J., & Stasyszyn, F. 2017, MNRAS, 472, 514, doi: 10.1093/mnras/stx1996

Hartmann, L., & Kenyon, S. J. 1996, Annual Review of A&A, 34, 207, doi: 10.1146/annurev.astro.34.1.207

Hwang, H.-C., Ting, Y.-S., & Zakamska, N. L. 2022, MNRAS, 512, 3383, doi: 10.1093/mnras/stac675

Kashi, A., & Soker, N. 2011, MNRAS, 417, 1466, doi: 10.1111/j.1365-2966.2011.19361.x

Kley, W., & Nelson, R. P. 2012, Annual Review of A&A, 50, 211, doi: 10.1146/annurev-astro-081811-125523

Kruckow, M. U., Neunteufel, P. G., Di Stefano, R., Gao, Y., & Kobayashi, C. 2021, ApJ, 920, 86, doi: 10.3847/1538-4357/ac13ac

Lacour, S., Biller, B., Cheetham, A., et al. 2016, A&A, 590, A90, doi: 10.1051/0004-6361/201527863

Lau, M. Y. M., Hirai, R., González-Bolívar, M., et al. 2022a, MNRAS, 512, 5462, doi: 10.1093/mnras/stac049
Lau, M. Y. M., Hirai, R., Price, D. J., & Mandel, I. 2022b, MNRAS, 516, 4669, doi: 10.1093/mnras/stac2490
Long, F., Andrews, S. M., Vega, J., et al. 2021, ApJ, 915, 131, doi: 10.3847/1538-4357/abff53
Lubow, S. H., & D'Angelo, G. 2006, ApJ, 641, 526, doi: 10.1086/500356
Mathieu, R. D., Stassun, K., Basri, G., et al. 1997, AJ, 113, 1841, doi: 10.1086/118395
Mignon-Risse, R., Oliva, A., González, M., Kuiper, R., & Commerçon, B. 2023, A&A, 672, A88, doi: 10.1051/0004-6361/202243514
Mohamed, S., & Podsiadlowski, P. 2012, Baltic Astronomy, 21, 88, doi: 10.1515/astro-2017-0362
Moody, M. S. L., Shi, J.-M., & Stone, J. M. 2019, ApJ, 875, 66, doi: 10.3847/1538-4357/ab09ee
Muñoz, D. J., & Lai, D. 2016, ApJ, 827, 43, doi: 10.3847/0004-637X/827/1/43
Muñoz, D. J., Lai, D., Kratter, K., & Miranda, R. 2020, ApJ, 889, 114, doi: 10.3847/1538-4357/ab5d33
Offner, S. S. R., Moe, M., Kratter, K. M., et al. 2022, The Origin and Evolution of Multiple Star Systems, doi: 10.48550/arXiv.2203.10066
Pakmor, R., Springel, V., Bauer, A., et al. 2016, MNRAS, 455, 1134, doi: 10.1093/mnras/stv2380
Passy, J.-C., De Marco, O., Fryer, C. L., et al. 2012, ApJ, 744, 52, doi: 10.1088/0004-637X/744/1/52
Price, D. J., Cuello, N., Pinte, C., et al. 2018, MNRAS, 477, 1270, doi: 10.1093/mnras/sty647
Pringle, J. E. 1991, MNRAS, 248, 754, doi: 10.1093/mnras/248.4.754
Ragusa, E., Alexander, R., Calcino, J., Hirsh, K., & Price, D. J. 2020, MNRAS, 499, 3362, doi: 10.1093/mnras/staa2954
Ramírez-Tannus, M. C., Kaper, L., de Koter, A., et al. 2017, A&A, 604, A78, doi: 10.1051/0004-6361/201629503
Ramírez-Tannus, M. C., Poorta, J., Bik, A., et al. 2020, A&A, 633, A155, doi: 10.1051/0004-6361/201935941
Ramírez-Tannus, M. C., Backs, F., de Koter, A., et al. 2021, A&A, 645, L10, doi: 10.1051/0004-6361/202039673
Reichardt, T. A., De Marco, O., Iaconi, R., Tout, C. A., & Price, D. J. 2019, MNRAS, 484, 631, doi: 10.1093/mnras/sty3485
Ricker, P. M., & Taam, R. E. 2012, ApJ, 746, 74, doi: 10.1088/0004-637X/746/1/74
Ricker, P. M., Timmes, F. X., Taam, R. E., & Webbink, R. F. 2019, IAU Symposium, 346, 449, doi: 10.1017/S1743921318007433
Roedig, C., Dotti, M., Sesana, A., Cuadra, J., & Colpi, M. 2011, MNRAS, 415, 3033, doi: 10.1111/j.1365-2966.2011.18927.x
Röpke, F. K., & De Marco, O. 2023, Living Reviews in Computational Astrophysics, 9, 2, doi: 10.1007/s41115-023-00017-x
Sana, H., Ramírez-Tannus, M. C., de Koter, A., et al. 2017, A&A, 599, L9, doi: 10.1051/0004-6361/201630087
Sesana, A., & Khan, F. M. 2015, MNRASL, 454, L66, doi: 10.1093/mnrasl/slv131
Shakura, N. I., & Sunyaev, R. A. 1973, A&A, 24, 337. https://ui.adsabs.harvard.edu/abs/1973A&A....24..337S
Shi, J.-M., Krolik, J. H., Lubow, S. H., & Hawley, J. F. 2012, ApJ, 749, 118, doi: 10.1088/0004-637X/749/2/118
Shu, F. H., Tremaine, S., Adams, F. C., & Ruden, S. P. 1990, ApJ, 358, 495, doi: 10.1086/169003
Siwek, M., Weinberger, R., & Hernquist, L. 2023a, MNRAS, 522, 2707, doi: 10.1093/mnras/stad1131
Siwek, M., Weinberger, R., Muñoz, D. J., & Hernquist, L. 2023b, MNRAS, 518, 5059, doi: 10.1093/mnras/stac3263
Smallwood, J. L., Lubow, S. H., & Martin, R. G. 2022, MNRAS, 514, 1249, doi: 10.1093/mnras/stac1416
Springel, V. 2010, MNRAS, 401, 791, doi: 10.1111/j.1365-2966.2009.15715.x
Stevenson, S., Vigna-Gómez, A., Mandel, I., et al. 2017, Nat Commun, 8, 14906, doi: 10.1038/ncomms14906
Tang, Y., MacFadyen, A., & Haiman, Z. 2017, MNRAS, 469, 4258, doi: 10.1093/mnras/stx1130
Tiede, C., & D'Orazio, D. J. 2023, Eccentric Binaries in Retrograde Disks, arXiv. https://arxiv.org/abs/2307.03775
Tiede, C., Zrake, J., MacFadyen, A., & Haiman, Z. 2020, ApJ, 900, 43, doi: 10.3847/1538-4357/aba432
Tofflemire, B. M., Mathieu, R. D., Herczeg, G. J., Akeson, R. L., & Ciardi, D. R. 2017, ApJ, 842, L12, doi: 10.3847/2041-8213/aa75cb
Tokovinin, A. 2020, MNRAS, 496, 987, doi: 10.1093/mnras/staa1639
Tokovinin, A., & Moe, M. 2020, MNRAS, 491, 5158, doi: 10.1093/mnras/stz3299
Trani, A. A., Rieder, S., Tanikawa, A., et al. 2022, Physical Review D, 106, 043014, doi: 10.1103/PhysRevD.106.043014
Tuna, S., & Metzger, B. D. 2023, Long-Term Evolution of Massive-Star Post-Common Envelope Circumbinary Disks and the Environments of Fast Luminous Transients, arXiv. https://arxiv.org/abs/2306.10111
Ward, W. R. 1997, ApJ, 482, L211, doi: 10.1086/310701
Zrake, J., & MacFadyen, A. I. 2012, ApJ, 744, 32, doi: 10.1088/0004-637X/744/1/32
Zrake, J., Tiede, C., MacFadyen, A., & Haiman, Z. 2021, ApJL, 909, L13, doi: 10.3847/2041-8213/abdd1c

APPENDIX

A. TABLES OF DERIVATIVES

We report here for convenience the tables of derivatives that were used for the interpolation, as described in Section 2.

q \ e	0.0	0.1	0.2	0.3	0.4	0.5	0.6	0.8
0.1	-1.28	-5.06	1.03	3.43	3.74	4.0	3.0	-6.32
0.2	-0.77	-1.51	-0.16	0.92	2.87	2.59	-1.3	-7.09
0.3	1.15	-2.05	-1.89	-0.19	-1.44	-0.93	-2.34	-3.49
0.4	1.29	-1.3	-0.65	-2.41	-2.5	-2.93	-1.48	-3.61
0.5	1.43	-0.69	-0.15	-2.43	-2.1	-3.73	-1.26	-3.52
0.6	1.58	-0.69	-0.42	-2.37	-2.96	-4.33	-0.3	-2.73
0.7	1.67	-0.75	-0.46	-2.38	-5.16	-4.36	0.28	-2.85
0.8	1.72	-0.94	-0.67	-2.52	-6.23	-0.28	0.52	-3.00
0.9	1.74	-0.88	-1.02	-4.15	-6.23	0.86	0.47	-2.89
1.0	1.76	-0.95	-1.31	-4.79	-6.10	0.60	0.38	-2.74

Table 1. Values of $\dot{a}/a$ in units of $\dot{M}/M$ from Siwek et al. (2023a)

q \ e	0.0	0.1	0.2	0.3	0.4	0.5	0.6	0.8
0.1	0.0	1.55	0.78	-1.84	-4.15	-4.78	-5.95	-7.7
0.2	0.0	1.32	2.14	0.16	-2.02	-3.96	-4.62	-5.47
0.3	0.0	3.73	5.59	0.23	-0.40	-2.73	-3.95	-3.46
0.4	0.0	4.29	3.50	2.52	0.23	-1.64	-2.81	-2.61
0.5	0.0	4.33	3.75	3.38	1.33	-1.82	-2.37	-2.15
0.6	0.0	4.73	4.90	4.52	3.33	-0.04	-2.20	-1.96
0.7	0.0	4.88	5.48	5.26	5.60	0.58	-2.14	-1.86
0.8	0.0	5.28	5.95	5.97	6.48	-1.15	-2.08	-1.70
0.9	0.0	5.16	6.60	8.33	7.02	-1.83	-2.12	-1.69
1.0	0.0	5.33	7.07	9.43	6.91	-1.67	-2.11	-1.85

Table 2. Values of $\dot{e}$ in units of $\dot{M}/M$ from Siwek et al. (2023a)

q \ e	0.0	0.2	0.4	0.6	0.8
0.1	6.51	4.55	2.00	1.24	1.34
0.2	3.94	7.05	2.16	1.60	1.51
0.3	3.05	4.82	2.67	1.84	1.97
0.4	2.28	3.43	3.19	3.30	1.30
0.5	2.03	3.41	4.79	3.33	9.26
0.6	1.86	3.21	4.08	1.88	8.60
0.7	1.63	2.96	1.97	1.35	8.56
0.8	1.40	2.51	1.64	1.13	8.97
0.9	1.17	2.22	1.29	1.09	9.91
1.0	1.00	1.00	1.00	1.00	1.00

Table 3. Values of λ from Siwek et al. (2023b).

e	$\dot{a}/a$	$\dot{e}$	e	$\dot{a}/a$	$\dot{e}$	e	$\dot{a}/a$	$\dot{e}$
0.000	2.23	0.00	0.300	-4.38	6.85	0.600	-0.41	-3.16
0.025	2.23	-0.36	0.325	-5.19	5.85	0.625	-0.72	-3.17
0.050	2.09	-0.55	0.350	-4.93	5.75	0.650	-1.00	-3.13
0.075	1.51	-0.61	0.375	-4.67	4.02	0.675	-1.35	-3.05
0.100	0.90	2.32	0.400	-4.06	2.65	0.700	-1.52	-3.01
0.125	0.04	2.92	0.425	-3.25	1.30	0.725	-1.67	-2.85
0.150	-0.51	5.10	0.450	-1.85	-0.55	0.750	-1.87	-2.65
0.175	-0.95	4.88	0.475	-0.40	-2.69	0.775	-2.22	-2.51
0.200	-1.09	4.36	0.500	0.17	-2.80	0.800	-2.73	-2.35
0.225	-1.80	4.42	0.525	0.07	-2.96			
0.250	-2.57	6.55	0.550	-0.15	-3.09			
0.275	-3.88	6.48	0.575	-0.24	-3.14			

Table 4. Values of $\dot{a}/a$ and $\dot{e}$ in units of $\dot{M}/M$ from Zrake et al. (2021).